Received 7 October 2023; accepted 10 November 2023. Date of publication 16 November 2023; date of current version 30 January 2024.

Digital Object Identifier 10.1109/OJAP.2023.3333800

A Slot-Connected Cavity Design With Corresponding Equivalent Circuit Model Analysis for Fully Metallic 3-D Vivaldi Antenna for Wireless Power Telemetry Applications

SUNANDA ROY (Graduate Student Member, IEEE), KARTHIK KAKARAPARTY (Graduate Student Member, IEEE), AND IFANA MAHBUB (Senior Member, IEEE)

Department of Electrical and Computer Engineering, The University of Texas at Dallas, Richardson, TX 75080, USA

CORRESPONDING AUTHOR: I. MAHBUB (e-mail: Ifana.Mahbub@utdallas.edu)

This work was supported by the Defense Advanced Research Projects Agency (DARPA) under Grant W911NF-23-1-0029.

ABSTRACT This paper presents the design of fully metallic 3D Vivaldi antenna that can be used for wireless power transmission applications. The 3D antenna consists of 1) a tapered profile, 2) a rectangular cavity, and 3) a horizontal slot cut that is used as a transition between the cavity and the tapered profile. The proposed antenna design is fabricated using two distinct approaches, the first of which is a 3D metal additive manufacturing (AM scheme) with a sequential material layer addition technique. The second version is based on the CNC milling (CNCM) technique implemented by selectively removing material in a controlled way. The measured gain of the AM and CNCA-based 3D Vivaldi antenna is 4.95 dBi, and 5.70 dBi, respectively. The measured bandwidth (BW) of the AM-based 3D antenna is 4.70 GHz (fractional BW (FBW) of 52.86%), whereas the CNCM-based 3D antenna is 4.95 GHz (FBW of 56.73%). Measurement outcomes indicate that the CNCM version of the 3D Vivaldi antenna is $\sim 1.2x$ more effective than the AM version in terms of realized gain and can be used for metal-based antenna system power telemetry due to its high gain and wide operational bandwidth capability.

INDEX TERMS All-metal antenna, slot-connected cavity, 3D vivaldi antenna, CNC manufacture, additive manufacture, wireless power transfer (WPT), wireless power telemetry.

I. INTRODUCTION

IN THIS modern era of day-to-day electronics, antennas play a vital role due to their ability to integrate with active electronics for efficient wireless communication and power transfer applications. In recent years, a plethora of antenna designs have been proposed that facilitate the trade-offs between bandwidth, polarization purity, high gain, ultra-wide beam steering, and wireless power transfer capabilities. For instance, prior works investigated planar antenna designs, including modular antennas [1], [2], [3], balanced antipodal Vivaldi array [4], [5], and Bowtie antenna designs [6], [7], [8]. Designing an antenna with wide operational bandwidth and a high gain while being compact in size is a challenging task.

Vivaldi antenna is one such antenna that has the capability to meet these criteria [9]. Vivaldi antenna designs have shown good performance with respect to antenna gain while achieving a highly directional radiation beam [10], [11], [12], [13], [14]. The wireless power transfer (WPT) system can be powered by onboard electronic equipment or via control devices from the ground station. The remotely powered ground-based system or remotely piloted vehicle (RPV) requires reliable wireless connection and power telemetry for control. Several approaches have been proposed for designing various architectures of the Vivaldi antenna, the most common of which is the planar version implemented on a dielectric substrate [15], [16], [17]. Another reason for the high cost is the complex design using expensive dielectric substrates such as Roger RT/duroid. Several ways have been proposed for designing a Vivaldi antenna, but the most common is a planar structure printed on a dielectric substrate [18], [19], [20], [21]. Even though antennas

fabricated using these previously proposed methods have a high gain and a wide frequency range, they can be hard to feed and expensive to fabricate, especially when they are made of solid metal. Although planar antennas can achieve a compact design, there is always a trade-off between the gain and the bandwidth [11], [22], [23], [24]. Planar Vivaldi antennas are particularly appealing because they have the capability to provide a good impedance match and wide scanning range over a wide range of bandwidths for phased-array configurations [25]. Moreover, they exhibit a high degree of cross-polarization and are relatively thick [26]. Furthermore, they are often fabricated using expensive, time-consuming procedures such as electrical discharge machining. Dual-polarized Vivaldi antennas implemented with two orthogonal crossed printed circuit boards (PCB) provide good radiation performance at a lower cost [27], [28]. One primary disadvantage of planar Vivaldi antennas is that they can be relatively difficult to manufacture and require precision milling or etching processes to achieve the necessary accuracy and consistency in their design. This can make them more expensive to produce compared to other types of antennas, particularly at larger sizes. Planar antennas, due to their two-dimensional nature, may encounter limitations in realizing intricate three-dimensional structures. Achieving the desired performance characteristics, such as wide bandwidth and high gain, can be particularly challenging in larger planar antennas, where precision is crucial, especially when striving for high consistency in their production. 3D metal printing on the other hand offers the advantage of directly translating intricate 3D designs into physical structures with high precision and consistency. This technique can mitigate some of the challenges associated with traditional planar antenna manufacturing methods. Additionally, planar Vivaldi antennas may exhibit some undesirable sidelobe radiation patterns, which can reduce their overall efficiency and effectiveness in specific applications. However, these Vivaldi antenna designs are beneficial for radar and point-to-point communications as they are highly directional. Usually, horn, dielectric rob, or Vivaldi antennas are also used in the same applications area, but they are bulky in structure [27], [29], [30]. Many researchers have used a dielectric lens as a director to make the wave more directed, which increases the gain [31], [32]. The gain is greatly improved, but the antenna's overall length has increased. Based on several research works related to microstrip planar antenna designs, it is evident that planar antennas have poor radiation efficiency, and their gain is low due to their structural limitations, which are confined to 2D, unlike 3D antennas. Recently, 3D antennas have emerged as a solution to compact designs with enhanced antenna gain, and ultra-wide bandwidth while achieving a highly focused radiation beam. Some of these designs include dipoles and slots-based antennas [33], [34], balanced antipodal Vivaldi array (BAVA) [35], frequency-scaled ultra-wide spectrum elements (FUSE) [36], and so on. The aforementioned limitations of planar microstrip antennas have given rise

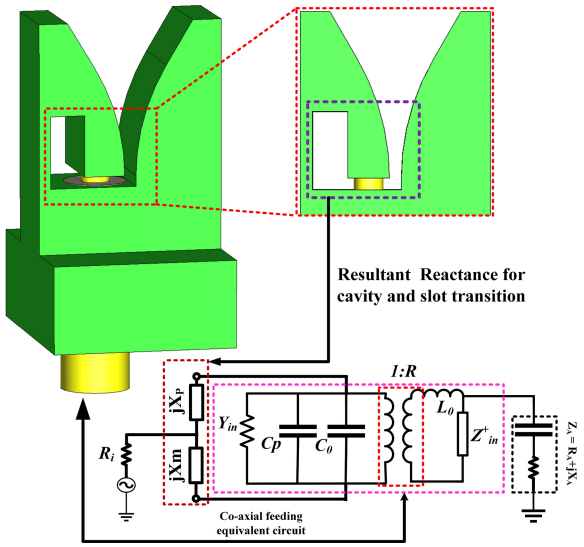

FIGURE 1. The proposed 3D Vivaldi antenna and identified different parts equivalent circuits.

to the development of high-precision 3D printed antennas using techniques such as additive manufacturing (AM) and computer numerical control manufacturing (CNCM) procedures. In particular, fully metallic 3D-printed antennas offer advantages in terms of precision and design flexibility for intricate antenna structures, which can result in higher performance. However, the initial investment in 3D metal printing equipment and materials may be higher. On the other hand, the PCB process may be more cost-effective for simpler antenna designs or larger production runs. Figure 1 shows the proposed 3D all-metal Vivaldi antenna and the corresponding equivalent circuit model. The novelty of this research is the design of a dielectric-free, simple, and compact 3D Vivaldi antenna, where (a) a tapered flare is designed based on an exponential equation that creates an opening in the middle of the antenna structure, which is directly connected with the slot line and helps in achieving the wide operational bandwidth, (b) a horizontal tapered cut in the middle facilitates the air gap from the cavity where the inner pin of the coaxial feeding connects with the main antenna part which improves the resonance of the antenna, (c) cutout a cavity from one half of the antenna is mainly responsible for the shifting of the resonance towards the centre frequency, and (d) equivalent circuit of the proposed antenna is developed, and demonstrates its validity using simulated performance.

This work presents two cost-effective all-metal 3D antenna versions that provide high gain, wide operational bandwidth, and highly directed radiation patterns. The rest of the paper is organized as follows: a detailed explanation of the geometrical view and corresponding equivalent circuit model are depicted in Section II. The two fabricated versions of the proposed antenna are discussed in Section III. The results and measurement discussion have been discussed in Section IV. The conclusion and future works are presented in Section V.

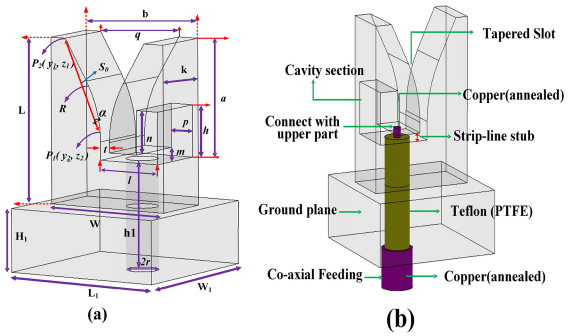

FIGURE 2. (a) Geometry, and corresponding (b) specification of different parts of the proposed 3D Vivaldi antenna.

II. PROPOSED ANTENNA GEOMETRY AND CORRESPONDING EQUIVALENT CIRCUIT MODEL

A. ANTENNA DESIGN AND ANALYSIS

The detailed geometry of the all-metal 3D antenna, as shown in Figure 2(a), is fabricated using aluminium metal based on two different fabrication approaches, such as AM and CNCM, respectively. The notations of the different dimensions of the proposed 3D Vivaldi antenna are shown in Figure 2(a), and the corresponding numerical values are listed in Table 1. These fabricated 3D Vivaldi antennas are apt for power telemetry and airborne UWB communications due to their compactness and high structural strength. The design parameters of the proposed antennas are shown in Figure 2(a). As shown in Figure 2(b), the coaxial feeding technique is used to feed the designed 3D Vivaldi antenna. The proposed shape can be classified into three categories: metallic parts (thickness, k), antenna grid parameters (vertical or H-plane spacing, L and horizontal or E-plane spacing, b), and antenna elementary parameters, which can be further subdivided into the strip-line transition, the tapered slot, and the cavity section. The strip-line transition is directly linked with the cavity portion, and the value of t is used to specify the width of the strip-line transition. The opening rate R and corresponding exponential taper profile are designed to define two points $P_1(y_1, z_1)$ and $P_2(y_2, z_2)$ by using the analytical curve tool of the computer simulation technology (CST). The exponential curve's starting and ending points P_1 (z_1,y_1) and P_2 (z_2, y_2) are expressed using the line equation of the opening rate (R) [37]. Here y_1 and z_1 are two exponential points for the taper line where (1) represents the exponential equation.

$$y = C_1 e^{Rz} + C_2$$
$$C_1 = \frac{y_2 - y_1}{e^{Rz_2} - e^{Rz_1}}$$
$$C_2 = \frac{y_1 e^{Rz_2} - y_2 e^{Rz_1}}{e^{Rz_2} - e^{Rz_1}} \quad (1)$$

The general solutions to the exponential equations are represented by the constants C_1 and C_2. The taper height a is $z_2 - z_1$ and the aperture height q is $2(y_2 - y_1)$. When R approaches zero, the exponential taper leads to a linearly tapered slot antenna (LTSA) in which the slope (S_0) of the taper is constant and expressed as $S_0 = (y_2 - y_1)/(z_2 - z_1)$. As depicted in equation (1), the slope of the exponential taper varies constantly between S_1 and S_2, where S_1 and S_2 are taper slopes at $z = z_1$ and at $z = z_2$, respectively, and at $S_1 < S < S_2$ for $R > 0$. The angle of the taper flare is expressed as $\alpha = \tan^{-1} S_0$. It is the slope of the taper line. The flare angles, on the other hand, depend on other parameters, such as a, b, and q, which denoted the height, width, and opening rate of the tapered slot of the maximum distance between the two halves of and the 3D antenna, respectively. The following parameters are related to the strip-line stub and cavity section, as shown in Figure 2(b). Moreover, t is the width of the tapered slot line, r is the radius of the coaxial feeding line, l is the length of the strip line stub, m is the height of the strip line stub, n is the length of the slot line cavity, p is the width of the slot line cavity, X_p is the reactive impedance of the cavity line, X_m is the reactive impedance of the strip line stub, and X_{GD} is the reactive impedance of the full ground plane. In this work, the width of the tapered slot (m) is fixed at 1 mm. The corresponding electrical equivalent circuit for the reference plane on the strip line is shown in Figure 3. The total impedance Z_T is the combination of strip line stub reactance $j(X_m)$ and the cavity reactance $j(X_p)$ that is connected in parallel with the antenna impedance Z_A. The shorting pin of the co-axial port is directly connected to the top part of the antenna, which creates a parallel connection between the cavity and the strip line.

TABLE 1. Optimized dimensions of the different parameters of the 3D Vivaldi antenna.

Parameter	Value (mm)	Parameter	Value (mm)
W	16	W_1	20
L	21	L_1	20
H	8	H_1	8
p	3	q	11.25
l	7	m	1
n	5.60	h	6.65
t	1.25	a	15
b	16	$2r$	5.5

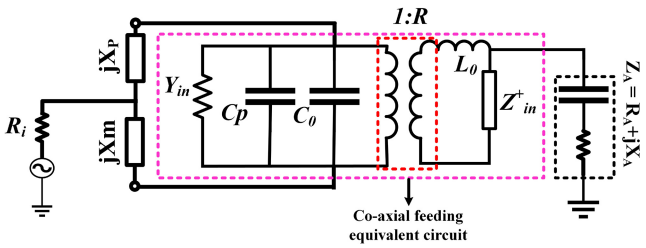

FIGURE 3. Proposed equivalent circuit of the 3D Vivaldi antenna.

B. DESIGN AND ANALYSIS OF THE EQUIVALENT CIRCUIT OF THE SLOT CONNECTED ANTENNA AND CORRESPONDING CO-AXIAL FEEDING

The equivalent circuit model is characterized by its intuitive nature, ease of processing, and minimal computational

TABLE 2. Optimized parameter of the proposed equivalent circuit.

Parameter	Value	Parameter	Value
X_p	0.25 pF	X_m	0.21 pF
Y_in	60 Ω	C_p	18 pF
C_0	46 pF	L_0	0.92 nH
$Ratio$	1 : 1	Z^+	600 Ω
X_A	4 pF	R_A	47 Ω

requirements. The identification of the model's parameters is straightforward and well-suited for conducting simulation tests using circuits. Hence, the use of the equivalent circuit model is prevalent in actual applications. The equivalent circuit of the proposed Vivaldi antenna is shown in Figure 3 and the corresponding parameter's optimized values are listed in Table 2. The equivalent circuit of the co-axial feeding is divided by the total reactance via the circuit model in Figure 3 [38]. The equivalent circuit of the co-axial feed is parallelly connected between the input and load sections. Capacitance due to parasitic inductance C_p is the capacitance from the probe barrel to the disconnected plate caused by higher-order modes, and it is solely dependent on the probe's geometry. It is independent of the size and shape of the Vivaldi antenna. It has a significant impact on the thickness of the substrate. The value of C_p varies as the substrate thickness varies, which impacts the first resonant frequency [39], [40]. The radius of the probe and the substrate thickness have a significant impact on the parasitic capacitance caused by the zero-order mode, which is denoted by C_0. There is no discernible fluctuation effect of C_0 on the resonant frequency or the return loss for the lower range of frequencies (0.5 to 20 GHz). Investigating the design evolution in terms of (a) 1^{st}, (b) 2^{nd}, and (c) 3^{rd} design steps of the proposed 3D antenna, it becomes apparent that at larger ranges of frequencies (above 20 GHz) which is not applicable in this work. Different parasitic effects, such as parasitic inductance caused by a zero-order mode L_0, work similarly as well. For example, there is no noticeable influence on the transformer R owing to variations in either the probe height or plate spacing h1 until the effect on the transformer becomes significant and hence not negligible at higher frequency ranges. The zero-order parasitic inductance L_0 of the feed probe has a significant effect on both the return loss and the resonant frequency. There are two major parameters that need to be investigated in order to understand how this inductance works. The first is the influence of the greater probe height h_1, and the second is the effect of the outer radius r. Probe height linearly increases the inductance L_0. Moreover, a longer probe produces a larger C_p but a smaller C_0 in terms of height. The return loss was further enhanced by the increased values of L_0, C_p, and C_0. During the simulation, two major issues were identified as the height of the probe increased. The first is that the return loss increases significantly in the CST modelling. The second is that the radiation patterns suffer greatly, as the radiation pattern deterioration is noticeable in CST simulation with a major dip on the primary axis ($\theta = 0°$ for broadside). The admittance Y_0 is indicative of the admittance caused by the propagating or zero-order mode. For single-element antenna analysis, Knorr's equivalent circuit model has been used to further match the antenna impedance Z_A into a transformer followed by parallel-connected slot lines terminated by the cavity slot and the radiating tapered slot [41], [42]. In order to do an analysis of both the full structure and the strip line structure without slots, The ground-plane impedance Z_T and the total stub reactance $j(X_m+X_p)$ can be determined by using the method of momentum (MoM) solver in the CST software. This helps to determine the impedance of the ground plan. The equivalent circuit model has been validated by observing that the correct Z_A is computed in this manner for strip line stubs of various shapes and sizes. However, this approach has been found to be ineffective for quantitative analysis of wide-band antennas due to the significant interaction between the cavity slot and the tapered slot. The length and width of the rectangular cavity h and p are varied from 6 to 6.5 mm and 2 to 3 mm to achieve the antenna's maximum BW and optimum impedance matching. A Polytetrafluoroethylene (PTFE) dielectric material with a 2.05 mm radius and 24.5 mm length is directly connected with the part of the ground plane and the top structure that isolates the inner pin from direct contact with the ground and the other part of the antenna. Long-pin coaxial SMA is used to feed the antenna part underneath the ground plane. In order to avoid electrical contact, the dielectric material (PTFE), which surrounds the inner conductor of the coaxial cable, is inserted with the inner pin through the lower and top ridges, as shown in Figure 2(b). In order to prevent penetration beyond the cavity wall (i.e., forming a height of 6.65 mm from the slot-line cavity) for a 2 mm -radius port, the feeding assembly is pressed into position so that the 0.61 mm radius center pin touches the top part of the slot. Epoxy is used to connect the top and ground portions of the fabricated 3D Vivaldi antenna with a long-pin SMA connector. The slot line structure incorporated in the antenna design is responsible for achieving the UWB response. In order to mitigate the back-lobe gratings, the width of the slot (q) has been optimized according to the highest operating frequency ($\lambda/2$) (where λ is calculated based on the center frequency 8.5 GHz). The length of the slot line, R, which is near $\lambda/2$, and the metal thickness of approximately $\lambda/4$ are crucial factors responsible for achieving an ultra-wide bandwidth.

A sequence of evolutionary stages is depicted in Figure 4 to achieve the ultimate structure. In the first iteration (i.e., Figure 4(a)), the antenna features a tapered section whose growth rate is designed using equation (1), yielding an UWB −10 dB impedance bandwidth of 7.07 to 10.48 GHz (as shown in Figure 5 (a) (black curve)), which is quite deficient. In the second iteration, a horizontal slot is cut from the tapered hole's edge, creating an air gap between the main and ground portions of the 3D antenna. The resulting reflection

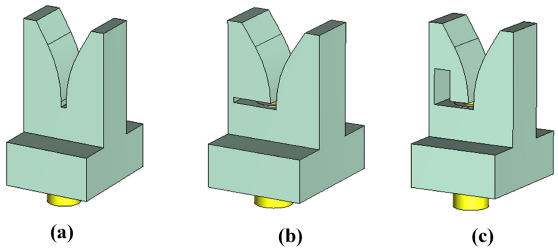

FIGURE 4. Investigated the design evolution in terms of (a) 1st, (b) 2nd, and (c) 3rd design steps of the proposed 3D antenna.

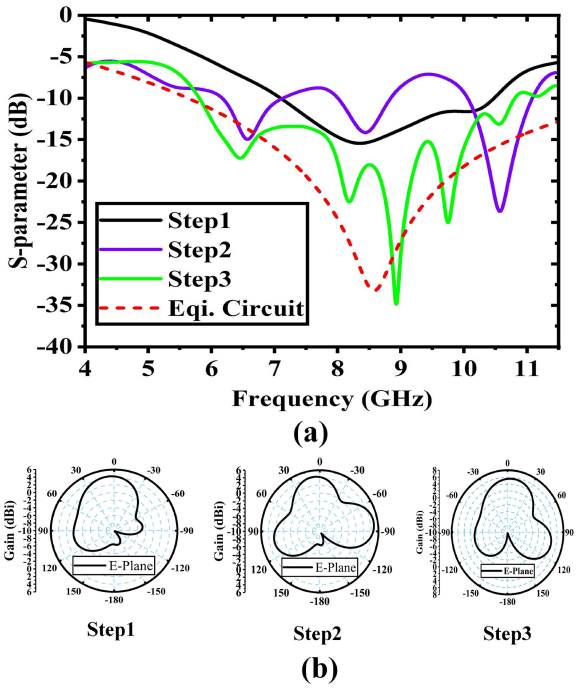

FIGURE 5. The reflection coefficient over the frequency for (a) different design steps and equivalent circuit, and (b) the corresponding radiation pattern.

coefficient is depicted in Figure 5(a) (purple curve). As can be seen, the value of the reflection coefficient is significantly improved (i.e., multiple resonances over the frequency range) due to the presence of the horizontal slot. The impedance BW is also expanded from 6.18 to 11.08 GHz compared to the 1st iteration, yet impedance matching is extremely poor (i.e., *RL* values are near −10 dB points at 6.5, 8.44, and 10 GHz, respectively. As a result, further modifications were made to the antenna during the 3st iteration, as shown in Figure 4(c), in order to attain UWB characteristics. To achieve broadband matching, the tapered slot line is loaded with a rectangular cavity. The length and width of the cavity, which act as a quarter wave matching circuit in conjunction with the slot line, impact the antenna's impedance. Additionally, the slot's tapering serves as a smooth impedance transition from the 50Ω feed to the free space wave impedance. The $S_{11} < -10$ dB bandwidth, demonstrating UWB ranging from 5.9 to 10.94 GHz as shown in Figure 5(a) (green curve). It matches the impedance very well over the frequency band. As a

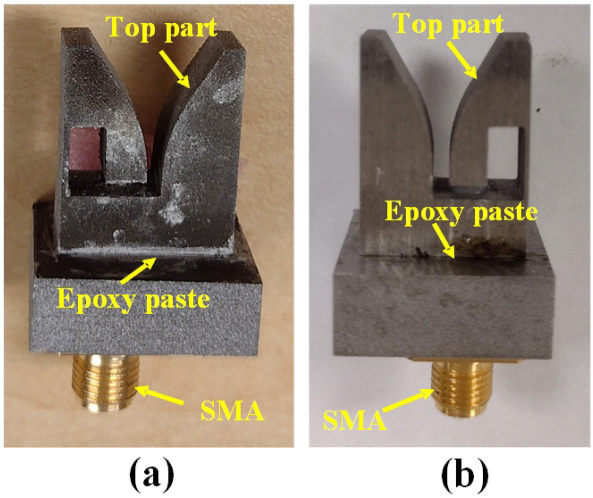

FIGURE 6. The fabricated versions of the proposed 3D antenna (a) additive version (b) milling version.

result, the antenna can cover the full UWB frequency range thanks to its resonating mode operating at 9 GHz and with a FBW of 52.86%. The *S*-parameter (red color) from the equivalent circuit matches perfectly with the final design of the proposed design. Similarly, the step-by-step evaluations in the proposed design with the corresponding *E*-field pattern are shown in Figure 5(b).

III. FABRICATION APPROACH

This section introduces the two cutting-edge manufacturing techniques employed to create the 3D Vivaldi antenna structures. The benefits and drawbacks of AM and CNCM processes are discussed with respect to fabrication cost, processing time, scalability, and dimensional accuracy.

A. THE AM-BASED 3D-ANTENNA FABRICATION

AM-based fabrication procedure involves the construction of 3D structures by gradually forming layers of the alloy under the supervision of a computer program. They are usually generated using digital data from a 3D model or electronic source file, such as a stereo-lithography (*STL*) file, which is one of the most common file types that 3D printers can read. The TruPr AM features are used for 3D printing, which can construct structures within a deposition area of 100 mm in diameter and 100 mm in height. Figure 6(a) depicts the prototype of the AM version of the proposed antenna.

B. THE CNCM BASED 3D-ANTENNA FABRICATION

The CNCM-based fabrication process involves the use of computers to manage the creation of complex parts from raw materials. This is the process of selectively removing material from a specialized workpiece using a cutting tool placed on a spinning spindle. CNCM machines can perform advanced functions like contouring surfaces and drilling holes with extreme precision. The cutting tool produces a series of rapid cuts on the raw material's surface, which are

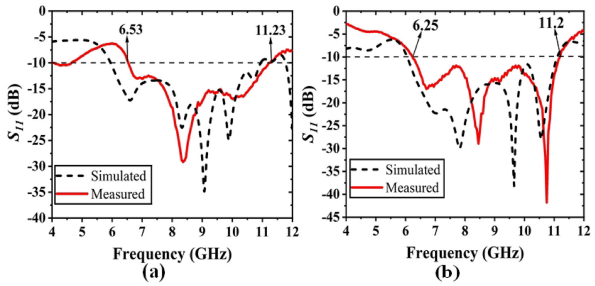

FIGURE 7. The simulated and measured S_{11} of the (a) AM and (b) CNCM versions of the all-metal 3D Vivaldi antenna.

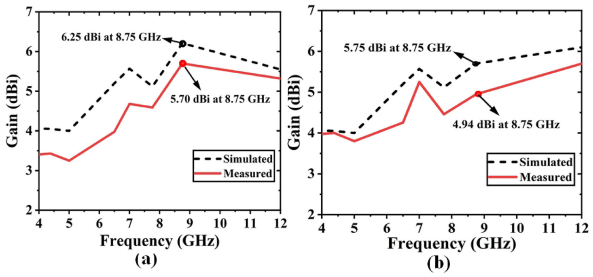

FIGURE 8. The simulated and measured realized gains of the (a) CNCM, and (b) AM versions of the 3D Vivaldi antenna.

gradually eliminated as the operation progresses. Figure 6(b) depicts the prototype of the CNCM version of the proposed antenna.

IV. SIMULATION AND MEASUREMENT RESULTS

In this work, aluminium metal is utilized to fabricate the 3D Vivaldi antennas. The frequency range considered is from 6 to 11 GHz with a center frequency of around 8.5 GHz, and the antenna is achieved 60% of fractional bandwidth. In both CNCM and AM processes, each part of the antenna is fabricated separately (top and bottom) to insert the SMA connector easily using J-B weld marine weld white epoxy adhesive paste. The original Cold Weld two-component epoxy system provides durable, long-lasting metal and surface rebuilding.

A. REFLECTION COEFFICIENT AND GAIN PERFORMANCE

The reflection coefficients, S_{11} of each version of the 3D Vivaldi antennas are measured using the ROHDE & SCHWARZ (R&S) ZVB-20 series Vector Network Analyzer (VNA). Figure 7(a) and 7(b) show the comparison between simulated and measured *RL* values of the CNCM and AM versions of the Vivaldi antennas. It can be seen that the simulated and the measured *RL* values are in comparatively excellent agreement. Though simulated and measured results are good in agreement there are some discrepancies between the two simulated results. There are two materials used to simulate the complete antenna for AM and CNCM processes, respectively. The aluminium titanium alloy (Ti-6AL) is used for the AM process, which has a composition of 90% titanium, 6% aluminium, 4% vanadium, 0.25% (maximum) iron, and 0.2% (maximum) oxygen, respectively. In the CNCM process, aluminium metal is used to fabricate the antenna, which material properties are different from aluminium titanium alloy. The same antenna is simulated using two different types of materials. That's why there are some discrepancies between the two simulated results. Figure 7(a) shows the measured value of the S_{11} of the CNCM version is less than −10 dB over the frequency range of 6.25 to 11.2 GHz, and it is −42.5 dB at 10.85 GHz. The simulated bandwidth (BW) of the milling version of the antenna is 5.25 GHz, which is 0.25 GHz higher than the measured value. Similarly, Figure 7(b) shows the comparison between the simulated and measured values of the *RL* of the AM version of the 3D antenna. The measured value of S_{11} of the AM version of the 3D antenna is less than −10 dB over the 6.53 to 11.23 GHz frequency range, and it is −28.5 dB at 8.75 GHz. The simulated bandwidth (*BW*) of the AM version is 5.58 GHz, which is 0.88 GHz higher than the measured value. The minor variations between the simulated and measured values of the *RL* and the *BW* of the CNCM and AM versions are due to the effect of epoxy paste that was used to make the contact with the SMA connector. The effect of the sensitivity of the SMA feeding point shows a slight difference in the number of resonant notches within the resonance *BW* of frequency of both antennas. Moreover, the cavity section beside the SMA helps to achieve the 50Ω impedance matching, which highly affects the *BW* of the antenna. Although the magnitudes of the *RL* of both versions of the 3D antennas are nearly similar, the S_{11} of the CNCM version is 14 dB less than the AM version. Due to the difference in material properties, such as electrical and thermal conductivity variations, dielectric constant, and diffusivity, the performance between the CNCM and AM versions shows some deviation. Figures 8(a) and 8(b) show the comparison between the simulated and measured realized gains of the CNCM and AM versions of the 3D antenna, respectively. For the CNCM version, the measured maximum gain at 8.75 GHz is 5.7 dBi, which is 0.55 dB less than the simulated value. The measured realized gain of the AM version is 4.94 dB at 8.75 GHz, which is 0.81 dBi less than the simulated gain. The measured gain of the CNCM version is 0.76 dBi higher than the AM version. It can be concluded that due to the pure aluminium's good conductivity, the CNCM version's gain performance is higher than the AM version. Figure 9(a), shows the simulated and measured total radiation efficiency of the proposed antenna. It can be seen that the maximum efficiency is 94.52% at 8.5 GHz frequency, whereas the efficiency at other ranges of the frequency band is below 90%. Similarly, Figure 9 (b) shows the axial ratio of the AM and CNCM versions of the proposed antenna. It can be seen that the axial at 7 GHz is 2.2, where the ratio of all other frequency bands is more

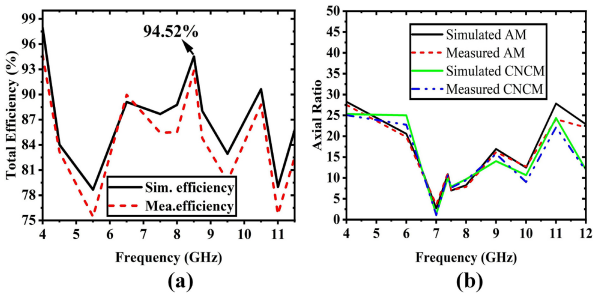

FIGURE 9. The comparison between simulated and measured (a) total efficiency, and (b) axial ratio of the proposed all-metal 3D Vivaldi antenna.

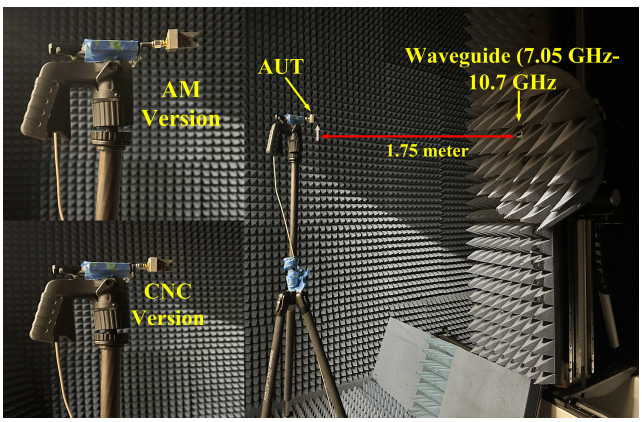

FIGURE 10. The set-up of the *NSI*2000 antenna measurement system for measuring the radiation pattern properties of the AM and CNC versions of the proposed 3D antenna.

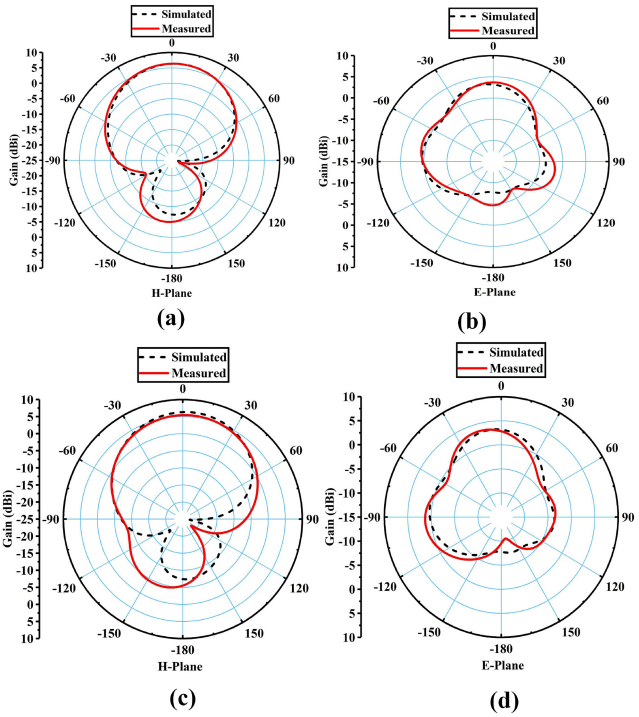

FIGURE 11. The simulated and measured radiation patterns of the 3D antenna at 8.75 GHz for the CNCM version (a) *X*-pol, (b) *Y*-pol, and additive version's (c) *X*-pol, (d) *Y*-pol.

than 3.Based on the axial ratio, the polarization properties at 7 GHz are circular, whereas all other frequency bands have elliptical polarization.

B. RADIATION PATTERN MEASUREMENT USING NSI2000 ANTENNA MEASUREMENT SYSTEM

Figure 10 depicts the experimental setup used to measure the radiation patterns of both versions of the proposed antennas. The *NSI*2000 measurement system is used to measure the CNCM and AM versions of the 3D antennas. It is a near-field antenna measurement system with model no $SOM-NSI2000-V4$. The frequency range of this system is 0 to 40 GHz. It provides fast and accurate methods of measuring the gain, directivity radiation pattern, etc. The NSI-RF-WR340 Waveguide (7.05 1−0.7 GHz) is used as a reference antenna that was placed 1.75 meters apart from the AUT (antenna under test). In Figure 11 (a), (b), (c), and (d), the simulated far-field radiation patterns of the proposed antenna are compared with the measured results for the azimuth (ϕ-axis) and elevation (θ-axis). The CNCM and AM versions simulated and measured radiation patterns are observed for the Y and X -pols for both ϕ and θ - axes, respectively. The half-power beam widths (HPBWs) of the CNCM version of the antenna at 8.75 GHz are 88.2° and 53.6° in the ϕ and θ- axises, respectively. Similarly, for the AM version, the HPBWs (Figure 11(c) and (d)) at 8.75 GHz in the ϕ and θ - axises are 85° and 52.7°, respectively. The HPBW of the CNCM version of the 3D antenna in the ϕ-axis is 3.2° smaller than the AM version due to the different material alloys used for manufacturing. On the other hand, the HPBW of the AM version of the 3D antenna in the θ -axis is 0.9° higher than the CNCM version. The side lob levels (SLL) of the radiation pattern of the CNCM version are −10.3 and −1.8 dB in the X and Y -pol, respectively. Similarly, the $SLLs$ of the radiation pattern of the AM version are −8.03 and −1.86 dB, respectively. Table 3 shows that the CNCM version performs better in terms of the gain, BW, and magnitude of reflection coefficient, whereas the AM version achieves a higher HPBW than the CNCM version. It should be noted that the cost of 3D antenna fabrication mainly depends on the quality alloy or powder. Based on the proposed fabrication process the total cost is 450 USD for both AM and CNCM versions. On the other hand, the cost of single-layer or multilayer PCB fabrication using Roger or Taconic is more than 1000 USD. Therefore, the 3D fabrication process is more cost-efficient than the PCB fabrication. Table 4 depicts the various performance parameters of the prior works related to the proposed all-metal 3D antennas. It can be observed that the proposed 3D antenna shows better performance in terms of gain, size, and radiation properties compared to the prior published works. As can be seen, the Φ and θ components (i.e., vertical and horizontal slots) of the 3D Vivaldi antenna are identical and vice versa. This illustrates how the only difference between the radiation characteristics of the two

TABLE 3. Achieved performances by the CNCM and AM versions of the 3D antenna.

Performance Parameters	CNCM version	AM version
Dimension (mm^3)	$20 \times 20 \times 29$	$20 \times 20 \times 29$
Gain (dBi)	5.70	4.94
BW (GHz)	4.95,	4.70,
Fractional BW (GHz)	0.56	0.52
Magnitude of Reflection Co-efficient	-42.5	-28.5
AM Version HPBW (ϕ and θ-axis)	55°	65°
CNCM Version HPBW (ϕ and θ-axis)	35°	60.25°
Cost	Low (150 USD)	High (300 USD)
Complexity	Simple procedure	High
Manufacturing time	2 to 4 hours	Approximately 24 hours

TABLE 4. Performance comparison with other state-of-the-art works.

Ref. No	**Dimension** (mm^3)	**Freq.**(GHz)	**BW**(GHz)	**Gain (dBi)**	**Material**	**Polarization**	**Efficiency**
[43]	$141 \times 131 \times 50$	$1.8 - 2.5$	0.7	$4.26 - 6.06$	$Al.$	Unidirectional	N/A
[44]	$420 \times 152 \times 20$	$3.75 - 4.15$	0.4	11.81	$Di.$	Unidirectional	73%
[45]	$45.3 \times 48 \times 5.2$	$2 - 6$	4	$1 - 6$	$M.$	Dual polarization	N/A
[46]	$232 \times 145 \times 0.508$	$0.7 - 2.7$	2	$4.05 - 8.3$	$Di.$	Uniform	80%
[47]	$131 \times 18 \times 2.5$	$0.5 - 9$	9.5	$-15 - 5$	$Al.$	Orthogonal	97%
[48]	$112 \times 18 \times 2.5$	$1.5 - 7.5$	6	5	$M.$	Bidirectional	90%
[49]	$59.1 \times 23.25 \times$ N/A	$0.28 - 5.91$	5.63	$-10, 16$	$M.$	Bidirectional	73%
Proposed	$20 \times 20 \times 29$	6.25 - 11.20 6.53- 11.23	4.95, 0.56 4.70, 0.52	5.70 4.94	$Al.$ Ti	Unidirectional	94.52%

$Al.^*$ = Aluminium, $M.^*$ = Metal, $Di.^*$ = Dielectric, $Ti.^*$ = Titanium

antennas is the variation in the properties of the materials. This is also due to the orthogonal alignment of two arms of the tapered slots of the antennas. The radiation pattern of the X-Pol looks more unidirectional than the pattern of the Y-pol. This is because the length of the cavity size is smaller than the strip line stub. It also contributes to the increase in directivity of the antenna. In [43], [44], [45], [46], [47], [48], [49], most of the performance parameters, such as dimension, BW, gain, and radiation efficiency, are lower than those of the proposed 3D Vivaldi antenna. Based on Table 4, the proposed work is better than some of the performance parameters, such as dimension, *BW*, and radiation efficiency, are better than some of the state-of-the-art works. In terms of the overall dimension, the proposed work is about $\sim 1.5x$ or more compact than all the state-of-the-art works in Table 4. The gain and BW of the proposed antennas are 4.94 and 5.70 dBi, and 4.75 and 4.95 GHz, which are better than the gain and *BW* of the state-of-the-art works [43], [47], [48], [49] and [43], [44], [45], [46], respectively. The radiation efficiency of the proposed work is greater than other prior works except [47]. Most of the prior works have designed all metal antennas based on the CNCM process using aluminium that was bulky in size. Though some of the prior works are better in terms of a few performance parameters, such as gain and *BW*, they are unsuitable for UAV-based applications due to the lack of compactness, UWB response, and high gain performance.

V. CONCLUSION

The paper proposes a compact all-metal 3D antenna with a rectangular cavity, tapered slot, and horizontal slot transition. The fabrication process using AM and CNCM techniques are compared. The results show that the CNCM-based fabricated 3D Vivaldi antenna achieves better performance than the AM version. The CNCM technique offers cost-effectiveness, fast and accurate manufacturing, and better precision in fabricating complex 3D structures compared to the AM process. The measured and simulated results match well. Future work involves the design of a 3D all-metal phased antenna array structure using the proposed 3D single antenna element and using CNCM, AM, and conventional manufacturing methods for comparison.

ACKNOWLEDGMENT

The authors would like to thank Dr. Narendra B. Dahotre, Founding Leader and Associate Vice President of the Center for Agile and Adaptive Additive Manufacturing (CAAAM), and his research student Dr. Mantri, Srinivas Aditya in the Materials Science Engineering Department of the University of North Texas for providing research facilities and technical support.

REFERENCES

[1] R. W. Kindt and B. T. Binder, "Dual-polarized planar-printed ultra-wideband antenna array on a triangular grid," *IEEE Trans. Antennas Propag.*, vol. 68, no. 8, pp. 6136–6144, Aug. 2020.

[2] S. S. Holland, D. H. Schaubert, and M. N. Vouvakis, "A 7-21 GHz dual-polarized planar ultrawideband modular antenna (PUMA) array," *IEEE Trans. Antennas Propag.*, vol. 60, no. 10, pp. 4589–4600, Oct. 2012.

[3] C. Pfeiffer, T. Steffen, G. Phillips, and B. Tomasic, "High power AESAs for 20-60 GHz with linear and circular polarizations," in *Proc. IEEE Int. Symp. Phased Array Syst. Technol. (PAST)*, 2019, pp. 1–4.

[4] M. W. Elsallal and J. C. Mather, "An ultra-thin, decade (10:1) bandwidth, modular"*BAVA*" array with low cross-polarization," in *Proc. IEEE Int. Symp. Antennas Propag. (APSURSI)*, 2011, pp. 1980–1983.

[5] J. Langley, P. Hall, and P. Newham, "Balanced antipodal Vivaldi antenna for wide bandwidth phased arrays," *IEEE Proc.-Microw. Antennas Propag.*, vol. 143, no. 2, pp. 97–102, 1996.

[6] S.-W. Qu, J.-L. Li, Q. Xue, and C.-H. Chan, "Wideband periodic endfire antenna with Bowtie dipoles," *IEEE Antennas Wireless Propag. Lett.*, vol. 7, pp. 314–317, 2008.

[7] K. Kakaraparty and I. Mahbub, "The design and SAR analysis of a UWB bow-tie antenna for wireless wearable sensors," in *Proc. U.S. Nat. Committee URSI Nat. Radio Sci. Meeting (USNC-URSI NRSM)*, 2022, pp. 204–205.

[8] H. Wong, K.-M. Mak, and K.-M. Luk, "Wideband shorted bowtie patch antenna with electric dipole," *IEEE Trans. Antennas Propag.*, vol. 56, no. 7, pp. 2098–2101, Jul. 2008.

[9] Z. Tahar, X. Dérobert, and M. Benslama, "An ultra-wideband modified Vivaldi antenna applied to through the ground and wall imaging," *Progr. Electromagn. Res. C*, vol. 86, pp. 111–122, Jan. 2018.

[10] Y. Chen, Y. He, W. Li, L. Zhang, S.-W. Wong, and A. Boag, "A 3-9 GHz UWB high-gain conformal end-fire Vivaldi antenna array," in *Proc. IEEE Int. Symp. Antennas Propagat. USNC-URSI Radio Sci. Meeting (APS/URSI)*, 2021, pp. 737–738.

[11] L. Sang, S. Wu, G. Liu, J. Wang, and W. Huang, "High-gain UWB Vivaldi antenna loaded with reconfigurable 3-D phase adjusting unit lens," *IEEE Antennas Wireless Propag. Lett.*, vol. 19, no. 2, pp. 322–326, Feb. 2020.

[12] P. Zhang and J. Li, "Compact UWB and low-RCS Vivaldi antenna using ultrathin microwave-absorbing materials," *IEEE Antennas Wireless Propag. Lett.*, vol. 16, pp. 1965–1968, 2017.

[13] M. Moosazadeh and S. Kharkovsky, "Development of the antipodal Vivaldi antenna for detection of cracks inside concrete members," *Microw. Opt. Technol. Lett.*, vol. 57, no. 7, pp. 1573–1578, 2015.

[14] P. A. Dzagbletey, J.-Y. Shim, and J.-Y. Chung, "Quarter-wave balun fed Vivaldi antenna pair for V2X communication measurement," *IEEE Trans. Antennas Propag.*, vol. 67, no. 3, pp. 1957–1962, Mar. 2019.

[15] Y. Pan, Y. Cheng, and Y. Dong, "Dual-polarized directive ultrawideband antenna integrated with horn and Vivaldi array," *IEEE Antennas Wireless Propag. Lett.*, vol. 20, no. 1, pp. 48–52, Jan. 2021.

[16] Y. Liu, W. Zhou, S. Yang, W. Li, P. Li, and S. Yang, "A novel miniaturized Vivaldi antenna using tapered slot edge with resonant cavity structure for ultrawideband applications," *IEEE Antennas Wireless Propagat. Lett.*, vol. 15, pp. 1881–1884, 2016.

[17] X. Shi, Y. Cao, Y. Hu, X. Luo, H. Yang, and L. H. Ye, "A high-gain antipodal Vivaldi antenna with director and metamaterial at 1–28 GHz," *IEEE Antennas Wireless Propag. Lett.*, vol. 20, no. 12, pp. 2432–2436, Dec. 2021.

[18] E. De Lera, E. Garcia, E. Rajo, and D. Segovia, "A coplanar Vivaldi antenna with wide band balun proposal for the low frequency band of the SKA: Approach to the FPA solution," in *Proc. IEEE Mediterr. Electrotechn. Conf.*, 2006, pp. 557–560.

[19] K. Ebnabbasi, D. Busuioc, R. Birken, and M. Wang, "Taper design of Vivaldi and co-planar tapered slot antenna (TSA) by Chebyshev transformer," *IEEE Trans. Antennas Propag.*, vol. 60, no. 5, pp. 2252–2259, May 2012.

[20] J. Langley, P. Hall, and P. Newham, "Novel ultrawide-bandwidth Vivaldi antenna with low crosspolarisation," *Electron. Lett.*, vol. 29, no. 23, pp. 2004–2005, 1993.

[21] Y. Wang, H.-T. Hsu, A. Desai, and Y.-F. Tsao, "Design of a compact RF front-end transceiver module for 5G new-radio applications," *IEEE Trans. Instrum. Meas.*, vol. 72, pp. 1–9, 2022, doi: 10.1109/TIM.2022.3229710.

[22] A. K. Singh, A. K. Dwivedi, V. Singh, and R. Yadav, "A miniaturized planar antenna with optimized slots and DGS for UWB applications," in *Proc. Int. Conf. Eng. Telecommun. (En&T)*, 2021, pp. 1–5.

[23] T. Roshna, U. Deepak, V. Sajitha, K. Vasudevan, and P. Mohanan, "A compact UWB MIMO antenna with reflector to enhance isolation," *IEEE Trans. Antennas Propag.*, vol. 63, no. 4, pp. 1873–1877, Apr. 2015.

[24] Y. Xiao, F. Yang, S. Xu, M. Li, K. Zhu, and H. Sun, "Design and implementation of a wideband 1-bit transmitarray based on a Yagi–Vivaldi unit cell," *IEEE Trans. Antennas Propag.*, vol. 69, no. 7, pp. 4229–4234, Jul. 2021.

[25] D. Schaubert and J. Shin, "Parameter study of tapered slot antenna arrays," in *IEEE Antennas Propagat. Soc. Int. Symp. Dig.*, vol. 3, 1995, pp. 1376–1379.

[26] P. M. Proudfoot, "A printed circuit folded dipole with integrated balun," Rome Air Develop. Center, Air Force Syst. Command, Rome, NY, USA, Rep. RADC TR-89-237, 1989.

[27] M. Sonkki, D. Sanchez-Escuderos, V. Hovinen, E. T. Salonen, and M. Ferrando-Bataller, "Wideband dual-polarized cross-shaped Vivaldi antenna," *IEEE Trans. Antennas Propag.*, vol. 63, no. 6, pp. 2813–2819, Jun. 2015.

[28] J. Zhang, E. C. Fear, and R. H. Johnston, "Cross-Vivaldi antenna for breast tumor detection," *Microw. Opt. Technol. Lett.*, vol. 51, no. 2, pp. 275–280, 2009.

[29] A. E.-C. Tan, K. Jhamb, and K. Rambabu, "Design of transverse electromagnetic horn for concrete penetrating ultrawideband radar," *IEEE Trans. Antennas Propag.*, vol. 60, no. 4, pp. 1736–1743, Apr. 2012.

[30] G. Adamiuk, T. Zwick, and W. Wiesbeck, "Compact, dual-polarized UWB-antenna, embedded in a dielectric," *IEEE Trans. Antennas Propag.*, vol. 58, no. 2, pp. 279–286, Feb. 2010.

[31] M. Moosazadeh, "High-gain antipodal Vivaldi antenna surrounded by dielectric for wideband applications," *IEEE Trans. Antennas Propag.*, vol. 66, no. 8, pp. 4349–4352, Aug. 2018.

[32] R. Cicchetti, V. Cicchetti, A. Faraone, L. Foged, and O. Testa, "A compact high-gain wideband lens vivaldi antenna for wireless communications and through-the-wall imaging," *IEEE Trans. Antennas Propag.*, vol. 69, no. 6, pp. 3177–3192, Jun. 2021.

[33] D. Cavallo, W. H. Syed, and A. Neto, "Connected-slot array with artificial dielectrics: A 6 to 15 GHz dual-pol wide-scan prototype," *IEEE Trans. Antennas Propag.*, vol. 66, no. 6, pp. 3201–3206, Jun. 2018.

[34] J. Zhong, A. Johnson, E. A. Alwan, and J. L. Volakis, "Dual-linear polarized phased array with 9:1 bandwidth and 60° scanning off broadside," *IEEE Trans. Antennas Propag.*, vol. 67, no. 3, pp. 1996–2001, Mar. 2019.

[35] M. W. Elsallal and J. C. Mather, "An ultra-thin, decade (10: 1) bandwidth, modular "BAVA" array with low cross-polarization," in *Proc. IEEE Int. Symp. Antennas Propagat. (APSURSI)*, 2011, pp. 1980–1983.

[36] R. W. Kindt, J. T. Logan, and M. W. Elsallal, "Machined metal FUSE array apertures," in *Proc. IEEE Int. Symp. Phased Array System Technol. (PAST)*, 2019, pp. 1–4.

[37] C. L. Prasanna, M. B. Lakshmi, and N. N. Sastry, "A parametric analysis & design of all metal Vivaldi antenna covering 3.0-18 GHz for DF and phased array applications," *Progr. Electromagn. Res. C*, vol. 92, pp. 57–69, Jan. 2019.

[38] Y.-J. Zhang and J. Fan, "An intrinsic circuit model for multiple vias in an irregular plate pair through rigorous electromagnetic analysis," *IEEE Trans. Microw. Theory Techn.*, vol. 58, no. 8, pp. 2251–2265, Aug. 2010.

[39] Y. Hu, Y. J. Zhang, and J. Fan, "Equivalent circuit model of coaxial probes for patch antennas," *Progr. Electromagn. Res. B*, vol. 38, pp. 281–296, Jan. 2012.

[40] M. Davidovitz and Y. Lo, "Input impedance of a probe-fed circular microstrip antenna with thick substrate," *IEEE Trans. Antennas Propag.*, vol. 34, no. 7, pp. 905–911, Jul. 1986.

[41] S. Gearhart, H. Ekstrom, P. Acharya, E. Kollberg, S. Jacobsson, and G. Rebeiz, "Submillimeter-wave endfire slotline antennas," in *IEEE Antennas Propag. Soc. Int. Symp. Dig.*, vol. 4, 1992, pp. 1898–1901.

[42] J. Knorr, "Slot-line transitions (short papers)," *IEEE Trans. Microw. Theory Techn.*, vol. 22, no. 5, pp. 548–554, May 1974.

[43] A. El-Bacha and R. Sarkis, "Design of tilted taper slot antenna for 5G base station antenna circular array," in *Proc. IEEE Middle East Conf. Antennas Propag. (MECAP)*, 2016, pp. 1–4.

[44] Y. Hou, Y. Li, Z. Zhang, and M. F. Iskander, "All-metal endfire antenna with high gain and stable radiation pattern for the platform-embedded application," *IEEE Trans. Antennas Propag.*, vol. 67, no. 2, pp. 730–737, Feb. 2019.
[45] Y. Chuo et al., "Design of a metal Vivaldi antenna with wide band and dual polarization," in *Proc. IEEE Int. Workshop Electromagn. Appl. Student Innov. Compet. (iWEM)*, vol. 1, 2021, pp. 1–3.
[46] Y. Dong, J. Choi, and T. Itoh, "Vivaldi antenna with pattern diversity for 0.7 to 2.7 GHz cellular band applications," *IEEE Antennas Wireless Propag. Lett.*, vol. 17, no. 2, pp. 247–250, Feb. 2018.
[47] R. W. Kindt and W. R. Pickles, "Ultrawideband all-metal flared-notch array radiator," *IEEE Trans. Antennas Propag.*, vol. 58, no. 11, pp. 3568–3575, Nov. 2010.
[48] E. G. Tianang, M. A. Elmansouri, and D. S. Filipovic, "Ultra-wideband lossless cavity-backed Vivaldi antenna," *IEEE Trans. Antennas Propag.*, vol. 66, no. 1, pp. 115–124, Jan. 2018.
[49] W. F. Moulder, K. Sertel, and J. L. Volakis, "Superstrate-enhanced ultrawideband tightly coupled array with resistive FSS," *IEEE Trans. Antennas Propag.*, vol. 60, no. 9, pp. 4166–4172, Sep. 2012.

SUNANDA ROY (Graduate Student Member, IEEE) received the B.Sc. degree in electronics and communication engineering from Khulna University, Bangladesh, the Master of Engineering degree in electrical and electronic engineering from the Khulna University of Engineering and Technology, Bangladesh, and the Ph.D. degree with the Faculty of Engineering, Multimedia University, Malaysia, under TM Research and Development Research Grant. He is currently working as a Postdoctoral Research Associate with the Department of Electrical and Computer Engineering, The University of Texas at Dallas. His research interests include ambient RF energy harvesting, hybrid harvesting, MIMO, multiband antenna design, integrated circuit design, and amplifier design.

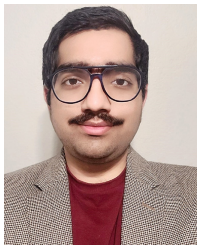

KARTHIK KAKARAPARTY (Graduate Student Member, IEEE) is currently pursuing the Ph.D. degree with the Electrical and Computer Engineering Department, The University of Texas at Dallas, USA, under the supervision of professor Dr. I. Mahbub. His current research focuses on antenna designs for millimeter wave applications and 5G technologies. Specifically, he has his interests aligned with designing highly focused beam-steering antenna arrays with ultrahigh gain and bandwidth for efficient drone-to-drone communications. His research interests also include the design of wearable and flexible antennas for on-body flexible electronics-based applications.

IFANA MAHBUB (Senior Member, IEEE) received the B.Sc. degree in electrical and electronic engineering from the Bangladesh University of Engineering and Technology in 2012, and the Ph.D. degree in electrical engineering from the University of Tennessee, Knoxville, in 2017. She is an Assistant Professor and the Texas Instrument's Early Career Chair Awardee of the Department of Electrical and Computer Engineering, The University of Texas at Dallas, where she is leading the Integrated Biomedical, RF Circuits and Systems Laboratory (iBioRFCASL). Her research interests include ultrawideband/mmwave phased-array antenna design for far-field wireless power transfer and vehicle-to-vehicle communication. She is the recipient of the NSF "Early Career Award" in 2020, and the DARPA "Young Faculty Award" in 2021. She serves as the Secretary for the URSI Commission K, and a Guest Editor for the IEEE OPEN JOURNAL OF ANTENNAS AND PROPAGATION and *Sensors* (MDPI).